Optimal Localizability Criterion for Positionning with DIstance-Deteriorated Relative Measurements

Accepted at the IEEE/RSJ IROS 2022 conference held in Kyoto, Japan.

The final version will be soon available in my author page https://ieeexplore.ieee.org/author/37086933423

Optimal Localizability Criterion for Positioning with Distance-Deteriorated Relative Measurements

Justin Cano[1,2], Gaël Pages[2], Eric Chaumette[2] and Jerome Le Ny[1]

***Abstract*— Position estimation in Multi-Robot Systems (MRS) relies on relative angle or distance measurements between the robots, which generally deteriorate as distances increase. Moreover, the localization accuracy is strongly influenced both by the quality of the raw measurements but also by the overall geometry of the network. In this paper, we design a cost function that accounts for these two issues and can be used to develop motion planning algorithms that optimize the localizability in MRS, i.e., the ability of individual robots to localize themselves accurately. This cost function is based on computing new Cramér Rao Lower Bounds characterizing the achievable positioning performance with range and angle measurements that deteriorate with increasing distances. We describe a gradient-based motion-planning algorithm for MRS deployment that can be implemented in a distributed manner, as well as a non-myopic strategy to escape local minima. Finally, we test the proposed methodology experimentally for range measurements obtained using ultra-wide band transceivers and illustrate the improvements resulting from leveraging the more accurate measurement model in the robot placement algorithms.**

I. Introduction

Reliable and accurate localization systems are critical for mobile robots to autonomously perform tasks in their environment. Various positioning technologies, e.g., short- and long-range radio-frequency (RF) systems, camera- or Lidar-based systems, offer different trade-offs in terms of performance, cost or applicability in various environments [1], [2]. Generally however, these technologies provide different modalities to obtain range or angle measurements between a robot and environmental features or between different robots in a Multi-Robot System (MRS).

The quality of the position estimates produced for an MRS based on relative range or angle measurements depends on the geometry of the network, a phenomenon known as *dilution of precision* [1, Chap. 7]. The relationship between network geometry and the ability of the robots to localize themselves can be captured through a *localizability cost function* [3], and the robots can then move to optimize this cost function and thus their positioning performance [3]–[6]. Localizability can be quantified independently of the localization scheme by using Cramér Rao Lower Bounds (CRLB), which provide a bound on the error covariance matrix of any unbiased position estimator one may implement in the MRS.

The CRLB depends on the specific stochastic error model considered for the raw distance or angle measurements. Although explicit CRLBs have been developed for measurement noise with constant variance [6], [7], in practice we observe for many systems that the quality of measurements degrades with distance. To address this issue, connectivity constraints can be added to maintain the robots sufficiently close [8], [9]. However, such constraints increase the complexity of the motion planning problems, and moreover this approach captures the issue of measurement quality only indirectly, leading to suboptimal geometries. Hence, in this paper we propose a measurement variance model with polynomial dependence on the robot inter-distances and derive the corresponding CRLB to be used to quantify localizability and develop MRS deployment algorithms.

To illustrate the usefulness of deriving more refined CRLBs and localizability measures, we focus on localization using Ultra-Wide Band (UWB) transceivers [10]. This technology can provide distance measurements with decimeter to centimeter-level accuracy [11] while being relatively inexpensive and energy efficient, which makes it particularly attractive for robotics applications [12]–[14], especially indoors. We consider the problem of localizing multiple robots equipped with UWB transceivers, called *tags*, communicating with each other and with other transceivers, called *anchors*, the location of the latter being known. Anchors can also be carried by mobile robots having access to an external source of localization. With enough relative distance or angle measurements obtained between the transceivers, the robot positions can be estimated for example using least-squares or filtering techniques [10], [15]. UWB sensors can acquire relative range [12], [14] or angle [16], [17] measurements, using a variety of protocols transmitting signals between nodes. The accuracy of these protocols deteriorates with the distance between transceivers because the received signal power decreases and errors due to fading and multi-path increase. In particular, the received signal power directly influences the *Leading Edge Detection* (LDE) algorithm used to estimate the signals' time-of-flight [10], [14]. Therefore, using a localizability criterion relying on the network's geometry without taking into account a realistic measurement error distribution can lead to misleading predictions about the tags' localization accuracy.

The rest of the paper is organized as follows. After a description of the problem in Section II, Section III presents the distance-dependent variance model for relative measure-

*This work was supported in part by FRQNT under grant 2018-PR-253646, by NSERC under grant RGPIN-5287-2018 and by the DGA/AID project 2019.65.0068.00.470.75.01.

[1] J. Cano and J. Le Ny are with the department of Electrical Engineering, Polytechnique Montréal and with GERAD, Montréal, QC, Canada. {justin.cano,jerome.le-ny}@polymtl.ca.

[2] J. Cano, G. Pages and E. Chaumette are with DEOS, ISAE-Supaéro, Toulouse, France. {gael.pages,eric.chaumette}@isae-suparero.fr.

ments and illustrates how to fit such a model experimentally for UWB range sensors. For this general polynomial variable model, the new localizability criterion is derived in Section IV, based on Fisher Information Matrices defining the CRLB, computed in Section V. Then, we present optimization algorithms in Section VI, which include gradient-descent based algorithms as well as non-myopic strategies to escape local minima. Finally, Section VII validates the methodology experimentally and illustrates the benefits of incorporating the refined model with distance deteriorated measurements to predict localization accuracy.

II. Problem Statement

Consider the problem of localizing in a given reference frame in dimension n, with $n = 2$ or 3, a set $\mathcal{U}$ of U tags with unknown positions, while relying on a set $\mathcal{K}$ of K anchors with known positions. Relative angle or range measurements $\mu_{ij} \in \mathbb{R}$ are available between a subset $\mathcal{E}$ of the tags and anchors, with $i \in \mathcal{U}$ and $j \in \mathcal{U} \cup \mathcal{K}$. Note that these measurements can involve either tag-tag or tag-anchor pairs, i.e., $\mathcal{E} \subset \mathcal{U} \times (\mathcal{U} \cup \mathcal{K})$. The coordinates $\mathbf{p}_i \in \mathbb{R}^n$ of node $i \in \mathcal{U} \cup \mathcal{K}$ in the reference frame are denoted $\mathbf{p}_i = [x_i, y_i, z_i]^\top$ if $n = 3$ or $\mathbf{p}_i = [x_i, y_i]^\top$ if $n = 2$. Each tag is assumed to be carried by a robot, and a subset $\mathcal{K}_M \subseteq \mathcal{K}$ of the anchors can also be mobile. Let $\mathbf{p} := [\dots \mathbf{p}_i^\top \dots]^\top \in \mathbb{R}^{nN}$ denote the positions of the $N := U + K$ nodes (anchors or tags).

A. Robot Placement Problem

We aim to move the robots to enhance the *localizability* of the tags, which is some measure of the accuracy with which we can compute an estimate $\hat{\mathbf{p}}_\mathcal{U}$ of the vector of tag positions $\mathbf{p}_\mathcal{U} := [\dots \mathbf{p}_i^\top \dots]^\top \in \mathbb{R}^{nU}$, $i \in \mathcal{U}$. Since the localizability depends on the network geometry $\mathbf{p}$, we introduce a *localizability function* $J(\mathbf{p})$, which takes smaller values when the achievable accuracy for $\hat{\mathbf{p}}_\mathcal{U}$ increases. We then aim to find the optimal geometry $\mathbf{p}^*$, solution to the following placement problem for the mobile nodes

$$\mathbf{p}^* = \underset{\{\mathbf{p}_j\}_{j \in \mathcal{K}_M \cup \mathcal{U}}}{\operatorname{argmin}} \; J(\mathbf{p}) + J_{\text{task}}(\mathbf{p}_\mathcal{U}), \tag{1}$$

where $J_{\text{task}}(\mathbf{p}_\mathcal{U})$ is an additional cost function that represents the tasks to be achieved by the robots carrying the tags. Indeed, from the tags' point of view, J can be seen as a constraint (*e.g.,* avoid configurations with poor localizability) as they must achieve tasks while been accurately localized. The function J should take into account both the geometry and the quality of the relative measurements μ_{ij}.

B. Distance-Deteriorating Measurement Models

The localizability depends on the assumed relative measurement model. In this paper, we consider the following Gaussian model

$$\mu_{ij} \sim \mathcal{N}\left(\bar{\mu}_{ij}(\mathbf{p}_{ij}), \sigma_{ij}^2(d_{ij})\right). \tag{2}$$

where $\bar{\mu}_{ij}$ is a mean function that depends on the relative positions $\mathbf{p}_{ij} := \mathbf{p}_i - \mathbf{p}_j$ of the pairs of agents $(i,j) \in \mathcal{E}$. The variance $\sigma_{ij}^2(d_{ij})$ of these measurements is a function of the inter-node distance $d_{ij} := ||\mathbf{p}_{ij}||$. Moreover, we assume that the measurements are independent for distinct pairs (i,j). This type of measurement model is standard for example for RF sensors estimating distances from Time-of-Flight (ToF) measurements [7], [13]. It is also used in 2D to model noise in Angle of Arrival (AoA) measurements [7], [16]. However, σ_{ij}^2 is generally assumed to be a constant, independent of the position, although in practice it is generally the case that the quality of the measurements decreases as the distance increases [7], especially as we approach the maximum range of a given technology. Hence, we propose to use variance functions $\sigma_{ij}^2(d_{ij})$ that model the degradation in measurement accuracy with distance, in order to improve the ability of the function $J(\mathbf{p})$ to accurately predict the localizability. It is important however to keep the computation of the function J and of its derivatives sufficiently simple in order to develop tractable motion planning algorithms.

III. Distance-Dependent Variance Model

In this section, we introduce a general polynomial model of the measurement variance $\sigma_{ij}^2(d_{ij})$ in (2). As an application, we calibrate a model of distance measurements with UWB transceivers.

A. Polynomial Variance Model

The proposed polynomial variance model is

$$\sigma_{ij}^2(d_{ij}; \boldsymbol{\alpha}) = \alpha_0 + \sum_{l=1}^{P} \alpha_l (d_{ij} - \delta_l)^l \mathbf{1}_{\delta_l < d_{ij}}. \tag{3}$$

where $P \in \mathbb{N}$ is the chosen degree of the polynomial and $\boldsymbol{\alpha} = [\alpha_0, \alpha_1, \delta_0, \dots, \alpha_P, \delta_P]^\top \in \mathbb{R}_+^{2P+1}$ is a vector of parameters. The the l-th order term of the polynomial activates at the distance δ_l. We assume that $\alpha_0 > 0$ because measurements are uncertain even at close range, and $\alpha_l \geq 0$ and $\delta_l \geq 0$, $\forall l \in [1, P]$, to keep $\sigma_{ij}^2(d_{ij}) > 0$ and increasing with distance. CRLBs are derived in [7] for the constant variance case where $P = 0$. The model (3) offers additional flexibility at long range while still allowing closed form expressions for the localizability function.

The parameter vector $\boldsymbol{\alpha}$ in (3) for a specific system and environment can be identified by collecting M measurements $\{\mu_{ij}^k(\mathbf{p}_{ij})\}_{k=1}^M$ at a set $\mathcal{M}$ of relative positions $\mathbf{p}_{ij}$, i.e., a total of $M \times |\mathcal{M}|$ measurements. We can then compute the empirical means $\hat{\bar{\mu}}_{ij}(\mathbf{p}_{ij}) = \frac{1}{M}\sum_{k=1}^M \mu_{ij}^k(\mathbf{p}_{ij})$ and variances $\hat{\sigma}_{ij}^2(\mathbf{p}_{ij}) = \frac{1}{M-1}\sum_{k=1}^M (\mu_{ij}^k(\mathbf{p}_{ij}) - \hat{\bar{\mu}}_{ij}(\mathbf{p}_{ij}))^2$, and finally obtain $\boldsymbol{\alpha}$ by solving the least squares problem

$$\boldsymbol{\alpha} = \underset{\check{\boldsymbol{\alpha}} \in \mathbb{R}_+^{2P+1}}{\operatorname{argmin}} \sum_{\mathbf{p}_{ij} \in \mathcal{M}} \left[\sigma_{ij}^2(||\mathbf{p}_{ij}||; \check{\boldsymbol{\alpha}}) - \hat{\sigma}_{ij}^2(\mathbf{p}_{ij})\right]^2. \tag{4}$$

B. Application to UWB Two-Way Ranging Measurements

To illustrate the model (3), we consider relative distance measurements acquired by two `Decawave DW1000` © UWB sensors [11] performing Single-Sided Two Way Ranging (SSTWR). The exact protocol to deduce distance measurements from signal time-of-flight measurements, including clock and power correction, is detailed in [14]. The

UWB transceiver j is carried by a mobile robot as shown on Fig. 1, and the transceiver i is fixed on a tripod. The robot moves to different positions while a motion capture system provides exact measurements of $\mathbf{p}_{ij}$. We compute empirical variances $\hat{\sigma}^2_{ij}(\mathbf{p}_{ij})$ using $M = 150$ measurement samples at each relative positions $\mathbf{p}_{ij}$. The results are plotted in Fig. 2 for a straight line trajectory, as a function of d_{ij}. A polynomial fit of the empirical variance is performed for $P = 3$ in (4) and shown in red.

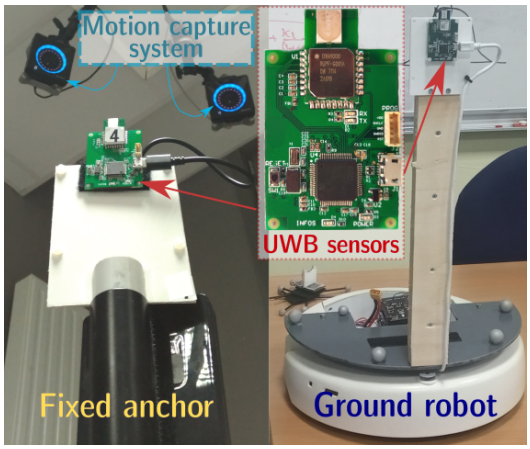

Fig. 1: Anchor, robot, motion capture system and UWB transceiver used for the variance model calibration.

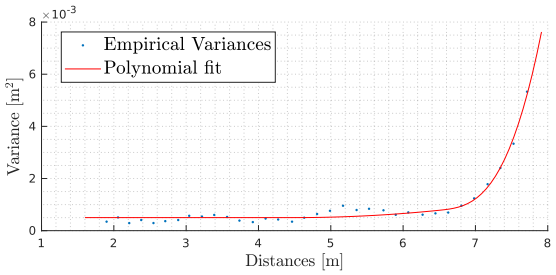

Fig. 2: Empirical variance and fitted polynomial.

At close range in Line-of-Sight (LoS) conditions, the received power is saturated, which can explain that the variance remains relatively constant. At longer range, the fact that received power theoretically decreases proportionally to the square of the distance could explain the parabolic shape of σ^2_{ij} when $d_{ij} > 6.5$ m. Moreover, even in LoS, outlier measurements can also be caused by multi-path propagation [10], [15], when reflected signals with significant power are detected by the LDE algorithm instead of the wave on the direct path. For our set-up using a wheeled robot and isotropic antennas, the planar ground leads to a higher chance of multi-path propagation as the distance increases. Note that the data collected to fit the model using (4) should include these outlier measurements, in order to capture such trends.

IV. Localizability Cost Function

As in [3], the cost function penalizing network geometries leading to poor localizability, i.e., poor accuracy of the estimator $\hat{\mathbf{p}}_\mathcal{U}$ of $\mathbf{p}_\mathcal{U}$, can be constructed from the CRLB. To define it, denote $f(\boldsymbol{\mu};\mathbf{p})$ the joint probability density function of the random measurement vector $\boldsymbol{\mu} = [\dots \mu_{ij} \dots]^\top$, which depends on the positions $\mathbf{p}$ of the tags and anchors. Moreover, assume that the estimator $\hat{\mathbf{p}}_\mathcal{U}$ is unbiased, *i.e.*, $\mathbb{E}\{\hat{\mathbf{p}}_\mathcal{U}\} = \mathbf{p}_\mathcal{U}$. Then, the covariance matrix $\Sigma_{\hat{\mathbf{p}}_\mathcal{U},\hat{\mathbf{p}}_\mathcal{U}}$ of $\hat{\mathbf{p}}_\mathcal{U}$ satisfies the CRLB [18, 3.3]

$$\Sigma_{\hat{\mathbf{p}}_\mathcal{U},\hat{\mathbf{p}}_\mathcal{U}} := \mathbb{E}\left\{(\hat{\mathbf{p}}_\mathcal{U} - \mathbf{p}_\mathcal{U})(\hat{\mathbf{p}}_\mathcal{U} - \mathbf{p}_\mathcal{U})^\top\right\} \succeq \mathbf{F}_\mathcal{U}^{-1}, \quad (5)$$

where $\mathbf{A} \succeq \mathbf{B}$ for symmetric matrices $\mathbf{A}, \mathbf{B}$ means that $\mathbf{A} - \mathbf{B}$ is positive semi-definite, and $\mathbf{F}_\mathcal{U} \in \mathbb{R}^{nU \times nU}$ is the Fisher Information Matrix (FIM), defined as follows [18, 3.7]

$$\mathbf{F}_\mathcal{U}(\mathbf{p}) = -\mathbb{E}_{\boldsymbol{\mu}}\left\{\frac{\partial^2 \ln f(\boldsymbol{\mu};\mathbf{p})}{\partial \mathbf{p}_\mathcal{U} \partial \mathbf{p}_\mathcal{U}^\top}\right\}. \quad (6)$$

Note that the FIM depends on the global geometry $\mathbf{p}$ and also on the specific distribution f of $\boldsymbol{\mu}$.

One can then define the localizability cost function to minimize as

$$J(\mathbf{p}) := \mathrm{Tr}\left\{\mathbf{F}_\mathcal{U}^{-1}(\mathbf{p})\right\}, \quad (7)$$

which is a lower bound on $\mathbb{E}\left\{\|\hat{\mathbf{p}}_\mathcal{U} - \mathbf{p}_\mathcal{U}\|^2\right\}$, the Mean Square Error (MSE) of $\hat{\mathbf{p}}_\mathcal{U}$. Using the CRLB has the advantage of providing a localizability measure that is independent of the specific estimator $\hat{\mathbf{p}}_\mathcal{U}$ implemented in the MRS. The function (7) corresponds to the A-Opt optimal design strategy [19, p.137], other functions can be used, such as $J_D(\mathbf{p}) = \log\det \mathbf{F}_\mathcal{U}^{-1}$ (D-Opt design) or $J_E(\mathbf{p}) = -\lambda_{\min}(\mathbf{F}_\mathcal{U})$ (E-Opt design, to maximize the minimum eigenvalue of $\mathbf{F}_\mathcal{U}$), as discussed in more detail in [20, III].

V. Computing the FIM

In this section we derive a closed form expression of the FIM $\mathbf{F}_\mathcal{U}$ for the measurement model introduced in sections II and III, which is required to evaluate the localizability function J in (7).

A. Structure of the FIM

The $nU \times nU$ FIM matrix $\mathbf{F}_\mathcal{U}$ can be decomposed into $n \times n$ blocks $\mathbf{F}_{ij}$, $1 \le i, j \le U$, written as

$$\mathbf{F}_{ij} = \begin{bmatrix} F_{ij}^{xx} & F_{ij}^{xy} & F_{ij}^{xz} \\ \star & F_{ij}^{yy} & F_{ij}^{yz} \\ \star & \star & F_{ij}^{zz} \end{bmatrix} \text{ or } \mathbf{F}_{ij} = \begin{bmatrix} F_{ij}^{xx} & F_{ij}^{xy} \\ \star & F_{ij}^{yy} \end{bmatrix}, \quad (8)$$

depending if $n = 3$ or $n = 2$, where $\star$ denotes symmetric terms. From the assumption that the measurements μ_{ij} are independent and only available for $(i,j) \in \mathcal{E}$, i.e., $f(\boldsymbol{\mu};\mathbf{p}) = \prod_{(i,j)\in\mathcal{E}} f_{ij}(\mu_{ij};\mathbf{p}_{ij})$, we deduce that $\mathbf{F}_{ij} = \mathbf{0}$ for $(i,j) \notin \mathcal{E}$, whereas for (i,j) pairs of tags in $\mathcal{E}$

$$F_{ij}^{\xi\eta} := -\mathbb{E}_{\mu_{ij}}\{\partial^2 \ln f_{ij}(\mu_{ij};\mathbf{p}_{ij})/\partial\xi_i \partial\eta_j\}, \quad (9)$$

where we denote pairs of Cartesian coordinates $\xi, \eta \in \{x,y,z\}^2$ if $n = 3$ or $\xi, \eta \in \{x,y\}^2$ if $n = 2$. We extend the expression (9) to tag-anchor pairs, so that $\mathbf{F}_{ij}$ is defined for all $(i,j) \in \mathcal{E}$. Then, we find that

$$\mathbf{F}_{ii} = -\sum_{j \in \mathcal{N}_i} \mathbf{F}_{ij},$$

where $\mathcal{N}_i = \{j \in \mathcal{U} \cup \mathcal{K}, (i,j) \in \mathcal{E}\}$, by using the fact that

$$\partial f_{ij}(\mu_{ij}; \mathbf{p}_{ij})/\partial \mathbf{p}_i = -\partial f_{ij}(\mu_{ij}; \mathbf{p}_{ij})/\partial \mathbf{p}_j.$$

Note that $\mathbf{F}_{ii}$ can require blocks $\mathbf{F}_{ij}$ outside $\mathbf{F}_{\mathcal{U}}$, *i.e.* when $j \in \mathcal{K}$. Hence, it is sufficient to obtain $\mathbf{F}_{\mathcal{U}}$ to compute the terms of (9) for all $(i,j) \in \mathcal{E}$. For the Gaussian measurement model (2), this can be done using the Slepian-Bangs Formula (SBF) [18, 3.9], which gives for $(i,j) \in \mathcal{E}$

$$F_{ij}^{\xi\eta} = \frac{\partial \bar{\mu}_{ij}}{\partial \xi_i}\frac{\partial \bar{\mu}_{ij}}{\partial \eta_j}\sigma_{ij}^{-2} + \frac{1}{2}\frac{\partial \sigma_{ij}^2}{\partial \xi_i}\frac{\partial \sigma_{ij}^2}{\partial \eta_j}\sigma_{ij}^{-4}. \tag{10}$$

We see that (10) involves the derivatives of the function σ_{ij}^2 defined in (3). For any $(i,j) \in \mathcal{E}$, coordinates $\xi_i \in \{x_i, y_i, z_i\}$, $\xi_j \in \{x_j, y_j, z_j\}$, and $\xi_{ij} = \xi_i - \xi_j$, we have

$$\frac{\partial \sigma_{ij}^2}{\partial \xi_i} = \partial \sigma_{ij}^2 := \sum_{l=1}^{P} \alpha_l \, l \, \frac{\xi_{ij}}{d_{ij}}(d_{ij} - \delta_l)^{l-1} 1_{\delta_l < d_{ij}}, \tag{11}$$

and $\partial \sigma_{ij}^2/\partial \xi_j = -\partial \sigma_{ij}^2/\partial \xi_i$. The expression $\partial \sigma_{ij}^2$ defined in (11) is zero if $P = 0$, i.e., if σ_{ij}^2 is constant. Note that at points such that $d_{ij} = \delta_l$, depending on the values of the constants α_l, (11) may only provide one-sided derivatives.

B. Distance Measurements

Suppose that the measurements are distances $\mu_{ij} = \tilde{d}_{ij}$ given by the model (2) with mean $\bar{\mu}_{ij} := ||\mathbf{p}_{ij}|| = d_{ij}$, so that $\partial \bar{\mu}_{ij}/\partial \xi_i = \xi_{ij}/d_{ij} = -\partial \bar{\mu}_{ij}/\partial \xi_j$. Starting from the SBF (10), using identity (11) and differentiation rules, we obtained for $(i,j) \in \mathcal{E}$

$$F_{ij}^{\xi,\eta} = -\frac{\xi_{ij}}{d_{ij}}\frac{\eta_{ij}}{d_{ij}}\sigma_{ij}^{-2}\left[1 + \frac{1}{2}\left(\partial \sigma_{ij}^2\right)^2 \sigma_{ij}^{-2}\right]. \tag{12}$$

with σ_{ij}^2 defined in (3) (we omitted the dependence on d_{ij} for conciseness), and the same notation for the coordinate $\eta \in \{x, y, z\}$ as for ξ. Alternatively, we can write for $(i,j) \in \mathcal{E}$

$$\mathbf{F}_{ij} = -\frac{w_{ij}}{\sigma_{ij}^2}\frac{\mathbf{p}_{ij}\,\mathbf{p}_{ij}^\top}{d_{ij}^2}, \tag{13}$$

where $w_{ij} := 1 + \frac{1}{2}\left(\partial \sigma_{ij}^2\right)^2 \sigma_{ij}^{-2}$.

Remark 1: The formulas in [7] correspond to (13) for a constant variance Gaussian model, i.e., $w_{ij} = 1$. As in [20], (13) can be used to establish a connection between the FIM and a weighted version of the *infinitesimal rigidity matrix* [21], which can be used to provide conditions guaranteeing the invertibility of $\mathbf{F}_{\mathcal{U}}$ [20, Theorem 2].

C. Angle Measurements

Suppose now that $n = 2$ and we have angle measurement $\mu_{ij} := \tilde{\theta}_{ij}$ between nodes $(i,j) \in \mathcal{E}$, with mean $\bar{\mu}_{ij} := \theta_{ij} := \angle(\vec{x}, \mathbf{p}_{ij})$, where $\vec{x}$ is a know reference direction. Without loss of generality, we choose $\vec{x} = [1, 0]^\top$, so that $\theta_{ij} = \text{atan2}(y_{ij}, x_{ij})$. For a coordinate variable $\xi \in \{x, y\}$, we denote by $\bar{\xi}$ the other coordinate. We also introduce the symbol $\mathsf{s}_{\xi,\eta}$, which is equals to 1 if $\eta = \xi$ and -1 if $\xi \neq \eta$. Finally, the SBF (10) yields directly the following formula, if $i \neq j$

$$F_{ij}^{\xi\eta} = -\frac{\bar{\xi}_{ij}}{d_{ij}}\frac{\bar{\eta}_{ij}}{d_{ij}}\sigma_{ij}^{-2}\left[\frac{\mathsf{s}_{\xi,\eta}}{d_{ij}^2} + \frac{1}{2}\left(\partial \sigma_{ij}^2\right)^2 \sigma_{ij}^{-2}\right]. \tag{14}$$

Alternatively, we can write for $(i,j) \in \mathcal{E}$

$$\mathbf{F}_{ij} = \sigma_{ij}^{-2}\left[-\frac{1}{2}\left(\partial \sigma_{ij}^2\right)^2 \sigma_{ij}^{-2}\frac{\mathbf{p}_{ij}\,\mathbf{p}_{ij}^\top}{d_{ij}^2} + \frac{\mathbf{B}_{ij}}{d_{ij}}\right], \tag{15}$$

where $\mathbf{B}_{ij} := d_{ij}^{-1}(\mathbf{I}_2 - \mathbf{p}_{ij}\mathbf{p}_{ij}^\top d_{ij}^{-2})$.

Remark 2: The matrices $\mathbf{B}_{ij}$ are 2×2 blocks of the *bearing rigidity matrix* as defined in [22, Theorem 8]. As in Remark 1, this link can be used to provide conditions guaranteeing the invertibility of $\mathbf{F}_{\mathcal{U}}$.

VI. Localizability Optimization Methods

In this section we discuss two motion strategies for the mobile nodes in $\mathcal{U}$ and $\mathcal{K}_M$ that improve localizability by minimizing the cost function J in (7).

A. Gradient Descent Strategy

To quickly improve the localizability of $\mathcal{U}$, we can use a gradient descent strategy starting from the initial configuration $\mathbf{p}^0$ of the network. For each agent $i \in \mathcal{U} \cup \mathcal{K}_M$, the successive desired positions are computed as follows

$$\mathbf{p}_i^{k+1} = \mathbf{p}_i^k - \eta \min\left\{1, \frac{\eta_{\max}}{||\partial J/\partial \mathbf{p}_i||}\right\}\frac{\partial J}{\partial \mathbf{p}_i}^\top\Bigg|_{\mathbf{p}_i = \mathbf{p}_i^k}, \tag{16}$$

where k denotes a step index, using a normalized stepsize rule [23]. The step size η is a given positive constant and $\eta_{\max}$ is a parameter adjusting the maximum distance $\eta_{\max}\eta$ between two iterations. The gradient $(\partial J/\partial \mathbf{p}_i)^\top$ can be computed using standard matrix differentiation rules [24], which give for each coordinate $\zeta_i \in \{x_i, y_i, z_i\}$, $i \in \mathcal{U} \cup \mathcal{K}_M$,

$$\frac{\partial J}{\partial \zeta_i} = -\text{Tr}\left\{\mathbf{F}_{\mathcal{U}}^{-2}\frac{\partial \mathbf{F}_{\mathcal{U}}}{\partial \zeta_i}\right\}. \tag{17}$$

In the Appendix, we provide an analytic formula for $\partial \mathbf{F}_{\mathcal{U}}/\partial \zeta_i$, which can also be used to evaluate gradients for cost functions J_D and J_E, from other optimal design strategies, see [3].

Suppose that the scheme (16) converges after l iterations to a configuration $\mathbf{p}^l$ in the neighborhood of a local minimum, i.e., $||\mathbf{p}_i^l - \mathbf{p}_i^{l-1}|| < \epsilon$ for each mobile node i and some threshold ϵ. The sequence of configurations $\{\mathbf{p}^k\}_{k=0}^l$ can be computed offline and used to provide a reference trajectory for a lower-level trajectory tracking controller. If used in real-time in a feedback loop however, the gradients in the scheme (16) can only be evaluated at the current estimates $\hat{\mathbf{p}}$, which are supposed unbiased.

The gradient descent scheme can also be implemented in a distributed manner by the nodes, i.e., it is possible for each node i to compute its local gradient $(\partial J/\partial \mathbf{p}_i)^\top$ in (16) by communicating only with its ranging neighbors. Indeed, the FIM has the same sparse structure as in [20], so that the distributed algorithms presented in Section V.B in that reference can be implemented.

B. Non-Myopic Localizability Improvement Policy

The gradient descent strategy can quickly improve the localizability of the MRS by finding a local minimum $\mathbf{p}^l$ of the function J. However, as we illustrate in Section VII, there may exist other configurations relatively close to $\mathbf{p}^l$ with significantly better localizability. Hence, we propose a search strategy to attempt to discover such configurations.

To do so, we introduce a regular grid of $\mathbb{R}^n$ around each $\mathbf{p}_i^l$, for $i \in \mathcal{U} \cup \mathcal{K}_M$. Starting from $\mathbf{p}^l$, we recursively construct the grid by allowing at each stage k motion vectors $\mathbf{u}_i^k \in \mathbb{R}^n$ for each mobile robot i, with components $\pm\delta$ for some step size δ, up to a maximum number of moves D. We associate a stage cost to a motion $\mathbf{u}_i^k$, which can penalize odometry drift, energy spent, etc. If we stop the robots in some configuration $\mathbf{p}^k$ at stage k, the terminal cost is $J(\mathbf{p}^k)$. We then compute via dynamic programming [25] trajectories for the robots that minimize the sum of the stage costs and the terminal cost, up to the maximum horizon D. The optimal trajectory found balances potential improvement in localizability with the total cost of the additional motions from $\mathbf{p}^l$.

Note that the complexity of the dynamic programming algorithm is polynomial in D, but exponential in the number of robots. It is also possible to reduce the size of the search space by removing from the grid the configurations $\mathbf{p}$ such that $J(\mathbf{p}) > (1+\gamma)J(\mathbf{p}^l)$ for some parameter $\gamma > 0$, which prevents trajectories to go through configurations for the MRS that deteriorate the localizability too much.

VII. Experimental Validation

To test the models and methods developed in this paper, we consider a simple scenario with 3 fixed UWB anchors $\mathcal{K} = \{K_1, K_2, K_3\}$, located at $\mathbf{p}_1 = [3.0, 2.0, 1.5]^\top$, $\mathbf{p}_2 = [3.0, -2.0, 1.5]^\top$ and $\mathbf{p}_3 = [-4, 0.1, 2.0]^\top$, and a unique UWB tag T carried by the robot shown on Fig. 1. The position of the tag is $\mathbf{p}_T = [x, y, z]^\top$ where $z = 0.43$ m is a fixed constant and $\mathbf{p}_\mathcal{U} := [x, y]^\top$ has to be determined. The tag T acquires distance measurements with the anchors using the SSTWR protocol described in [14], and we aim to find a position that optimizes its localizability.

The following model for the distance measurement variance is identified empirically in the area where the experiment is held, as explained in Section III

$$\sigma_{Tj}^2 = \alpha_0 + \alpha_2 (d_{Tj} - \delta_2)^2 \mathbf{1}_{\delta_2 < d_{Tj}}, \quad j \in \mathcal{K}, \tag{18}$$

where $\alpha_0 = 0.038^2$ m^2, $\alpha_2 = 5 \times 10^{-3}$ and $\delta_2 = 4.5$ m. To stress the benefits of using the model (18) for localizability optimization, we consider two deployment scenarios: first, using a Constant Variance (CV) model, as in [20], with $\alpha_0 = 0.1^2$ m^2, $\alpha_2 = 0$, and second using the Quadratic Variance (QV) model (18). Then, we compare the actual positioning performances and the localizability potential values for both trajectories to stress the benefits of the refined model.

The values of the cost $J(\mathbf{p}_\mathcal{U}) = \mathrm{Tr}\left\{\mathbf{F}_\mathcal{U}^{-1}(\mathbf{p}_\mathcal{U})\right\}$ for the CV and QV models are plotted on a logarithmic color scale on Fig. 3. Note that $\mathbf{F}_\mathcal{U}$ corresponds to the information on x and y coordinates but involves distance measurements in $\mathbb{R}^3$. The initial tag position is $\mathbf{p}_\mathcal{U}(0) = [-2.5, 0.5]^\top$. For the CV model, the cost presents minima that are quite far from the anchors, which ignores the deterioration of the the measurements with the distance. In contrast, the cost for the QV model has its global minimum inside the triangle formed by the anchors, which is an intuitive placement solution.

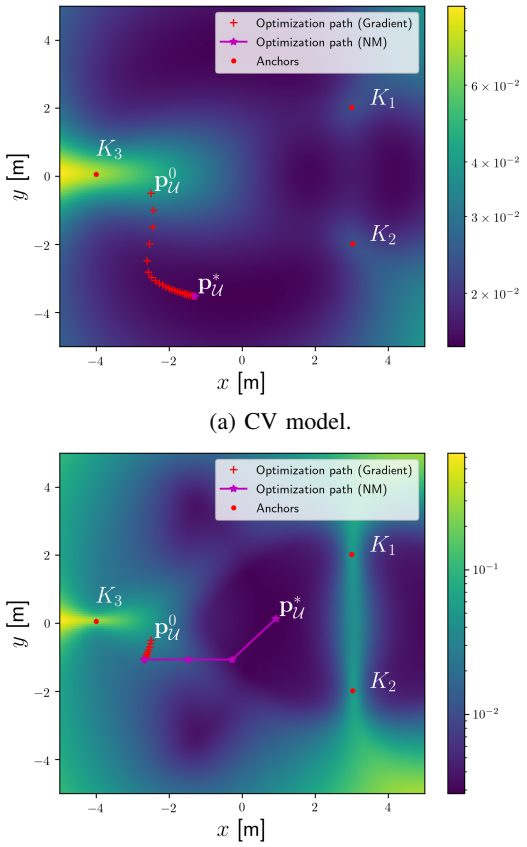

(a) CV model.

(b) QV model.

Fig. 3: 2D localizability cost $J(x, y)$ and computed paths for the tag, with the CV and QV models.

To move the tag and optimize the localizability cost J, for both scenarios we first use the gradient descent scheme (16). We set $\mathbf{p}_\mathcal{U}^0 := \mathbf{p}_\mathcal{U}(0)$, $\eta = 200$ and $\eta\eta_{\max} = 0.5$ m, and plot the computed paths in red on Fig. 3. After convergence, which is detected using a tolerance parameter $\epsilon = 0.1$ m, we apply the Non-Myopic (NM) optimization strategy of Section VI-B. We use a step size $\delta = 1.2$ m, a depth $D = 4$ and a stage cost equal to $2.0 \times 10^{-4} \times \|\mathbf{u}_T\|^2$. The NM strategy returns a path from $\mathbf{p}_\mathcal{U}^l$ to a potentially new point $\mathbf{p}_\mathcal{U}^*$ with better localizability, plotted in magenta on Fig. 3. However, in the CV case it turns out that $\mathbf{p}_\mathcal{U}^l$ was already a global minimum of the cost function, so that the NM optimization has no effect for that model.

Then, the robot follows pre-computed trajectories joining the waypoints $\{\mathbf{p}_\mathcal{U}^0, \ldots, \mathbf{p}_\mathcal{U}^l, \ldots, \mathbf{p}_\mathcal{U}^*\}$ and acquires along them UWB range measurements with the anchors. At each position $\mathbf{p}_\mathcal{U}(t)$, it measures distances $\tilde{d}_{Tj}$, $j \in \mathcal{K}$, and computes its position estimate by solving the least squares

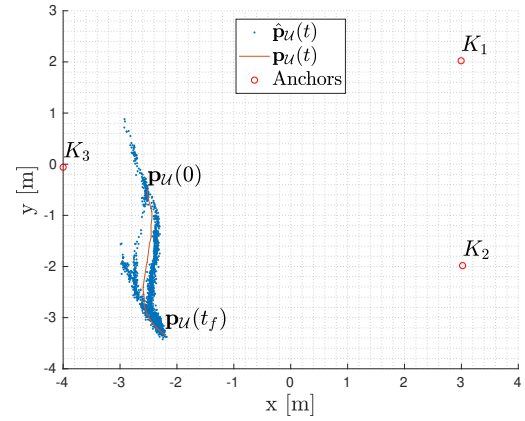

(a) CV model.

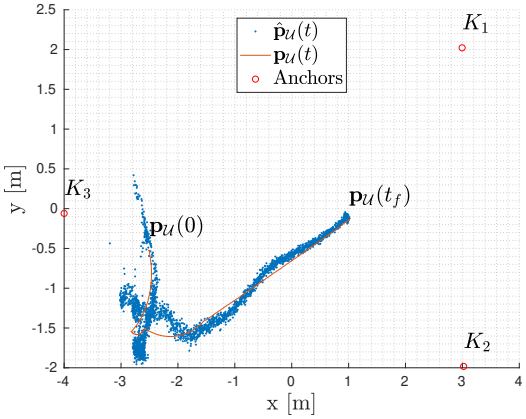

(b) QV model.

Fig. 4: Performed trajectory and robot position estimates.

problem

$$\hat{\mathbf{p}}_{\mathcal{U}}(t) = \underset{\mathbf{p}\in\mathbb{R}^2}{\operatorname{argmin}} \sum_{j\in\mathcal{K}} \left(\tilde{d}_{Tj}(t) - ||\mathbf{p} - \mathbf{p}_j(t)||\right)^2,$$

using the Gauss-Newton method [23]. A motion capture system records the true trajectory $\mathbf{p}_{\mathcal{U}}(t)$ of the robot. Since we are only interested here in characterizing the localization error, we use $\mathbf{p}_{\mathcal{U}}(t)$ directly to control the motion of the robot and follow the preplanned trajectory, instead of $\hat{\mathbf{p}}_{\mathcal{U}}(t)$. Finally, we compute the Squared Error (SE) $SE(t) = ||\mathbf{p}_{\mathcal{U}}(t) - \hat{\mathbf{p}}_{\mathcal{U}}(t)||^2$ and the potential $J(\mathbf{p}_{\mathcal{U}}(t))$. We plot the results on Figs. 4 and 5 for one trajectory. We also summarize in Table I the empirical MSE and 3σ confidence bounds for the initial and final position estimates in both scenarios over five trajectories.

During the first 3 seconds of each run, we observe large SE values, as shown on Fig. 5 and by the empirical MSE for $\mathbf{p}_{\mathcal{U}}(0)$ in Table I. The cost $J(\mathbf{p}_{\mathcal{U}})$ is correspondingly high, *i.e.*, the localizability is poor. Indeed, the cost function is a theoretical lower bound on the MSE, which is highlighted along the trajectories by the superposition of $J(\mathbf{p}_{\mathcal{U}}(t))$ and $SE(t)$ on Fig. 5. After about 4 seconds for both scenarios the localization error decreases as the robot moves. However, range measurement errors presumably due to multi-path are

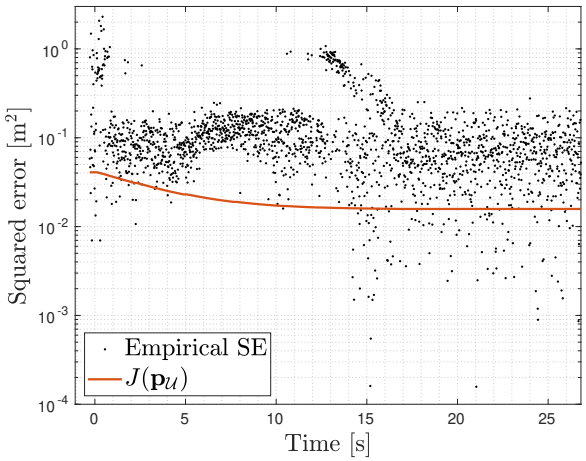

(a) CV scenario.

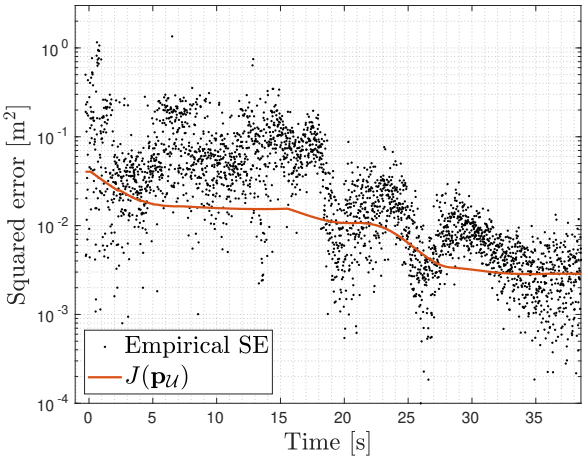

(b) QV scenario.

Fig. 5: Squared positioning error and localizability cost.

TABLE I: Empirical MSE for initial and final positions.

[m^2]	$\mathbf{p}_{\mathcal{U}}(0)$	$\mathbf{p}_{\mathcal{U}}(t_f)$ (CV)	$\mathbf{p}_{\mathcal{U}}(t_f)$ (QV)
MSE	0.38	0.23	8.3×10^{-3}
3σ	± 0.09	± 0.01	$\pm 0.46 \times 10^{-3}$

observed when the robot is moving and is far from the anchors K_1 and K_2 (see Fig. 5a after about 13 s for example), which yields a significant loss of precision. These distance-dependent deterioration issues with the measurements are ignored by the CV model, while using the QV model for deployment leads to a significant improvement of the MSE when the final position $\mathbf{p}^*_{\mathcal{U}}$ computed by the NM strategy is reached after 35 seconds.

VIII. Conclusion and Perspectives

In this paper, we developed a localizability criterion taking into account relative measurement distortion at long range, which provides a tighter bound on the covariance of position estimates compared to constant measurement error variance models. To use this criterion for robot deployment, we described gradient-based and non-myopic optimization

schemes. The possible improvements in positioning accuracy have been illustrated experimentally. Future work includes developing tractable non-myopic policies to search for optimal configurations over a larger area.

ACKNOWLEDGMENTS

The authors thank Corentin Chauffaut and Louis Treton from ISAE for their availability and their assistance.

APPENDIX

Here we give the expressions of $\partial \mathbf{F}_{ij}/\partial \mathbf{p}_l$ required to evaluate $\partial J/\partial \mathbf{p}_l$ in (16) via (17). Consider a coordinate $\zeta_l \in \{x_l, y_l, z_l\}$. If $i \neq j$, $\partial F_{ij}^{\xi\eta}/\partial \zeta_l = 0$ for all $l \notin \{i, j\}$. Next, if $i = j$ we have $\partial F_{ii}^{\xi\eta}/\partial \zeta_l = -\sum_{j \in \mathcal{N}_i \cap \mathcal{N}_l} \partial F_{ij}^{\xi\eta}/\partial \zeta_l$. Finally, since the FIM $\mathbf{F}_{\mathcal{U}}$ is symmetric, we have $\partial F_{ij}^{\xi\eta}/\partial \zeta_l = \partial F_{ji}^{\xi\eta}/\partial \zeta_l$. Therefore, to determine all the terms $\partial F_{ij}^{\xi\eta}/\partial \zeta_l$ of $\partial \mathbf{F}_{\mathcal{U}}/\partial \zeta_l$ it is sufficient to compute $\partial F_{lj}^{\xi\eta}/\partial \zeta_l$ for $j \in \mathcal{N}_l$.

We find

$$\frac{\partial F_{lj}^{\xi\eta}}{\partial \zeta_l} = -\frac{\partial r_{ij}}{\partial \zeta_l}\sigma_{lj}^{-2} q_{lj} + r_{ij}\zeta_{lj}(\partial \sigma_{lj}^2)\sigma_{ij}^{-4} q_{lj} - r_{ij}\sigma_{lj}^{-2}\frac{\partial q_{lj}}{\partial \zeta_l},$$

where $r_{ij} = \xi_{lj}\eta_{lj} d_{lj}^{-2}$ and $q_{lj} = w_{lj} = 1 + \frac{1}{2}\left(\partial \sigma_{lj}^2\right)^2 \sigma_{lj}^{-2}$ if we consider distance measurements or $q_{lj} = \frac{\mathsf{s}_{\xi,\eta}}{d_{ij}^2} + w_{ij} - 1$ for angle measurements. We then compute the two remaining derivatives $\partial r_{ij}/\partial \zeta_l$ and $\partial q_{lj}/\partial \zeta_l$. First, we have

$$\frac{\partial r_{ij}}{\partial \zeta_l} = d_{lj}^{-2}\gamma_{lj} - 2\xi_{lj}\eta_{lj}\zeta_{lj} d_{lj}^{-4},$$

where

$$\gamma_{lj} = \begin{cases} \xi_{lj} \text{ if } \zeta = \eta \text{ and } \xi \neq \eta, \\ \eta_{lj} \text{ if } \zeta = \xi \text{ and } \xi \neq \eta, \\ 2\zeta_{lj} \text{ if } \zeta \in \{\eta, \xi\} \text{ and } \xi = \eta, \\ 0 \text{ if } \zeta \notin \{\eta, \xi\}. \end{cases}$$

Second, if we consider distances measurement, we have

$$\frac{\partial q_{lj}}{\partial \zeta_l} = \frac{\partial w_{lj}}{\partial \zeta_l} = \frac{\zeta_{lj}}{2d_{lj}}\left(2(\partial^2 \sigma_{lj}^2)(\partial \sigma_{lj}^2)\sigma_{lj}^{-2} - (\partial \sigma_{lj}^2)^3 \sigma_{ij}^{-4}\right),$$

where

$$\partial^2 \sigma_{lj}^2 = \sum_{l=2}^{P} \alpha_l\, l\,(l-1)(d_{lj} - d_{0,l})^{l-2}\, \mathbf{1}_{d_{0,l} < d_{ij}},$$

and for angle measurements

$$\frac{\partial q_{lj}}{\partial \zeta_l} = -2\zeta_{lj}\frac{\mathsf{s}_{\xi,\eta}}{d_{ij}^3} + \frac{\partial w_{lj}}{\partial \zeta_l}.$$

REFERENCES

[1] P. D. Groves, *Principles of GNSS, inertial, and multisensor integrated navigation systems*, 2nd ed. Artech House, 2013.

[2] P. Corke, *Robotics, Vision and Control*, ser. Springer Tracts in Advanced Robotics, B. Siciliano and O. Khatib, Eds. Springer Berlin Heidelberg, 2011, vol. 73.

[3] J. Le Ny and S. Chauvière, "Localizability-Constrained Deployment of Mobile Robotic Networks with Noisy Range Measurements," in *2018 Annual American Control Conference (ACC)*, Jun. 2018, pp. 2788–2793.

[4] B. Irani, J. Wang, and W. Chen, "A Localizability Constraint-Based Path Planning Method for Autonomous Vehicles," *IEEE Transactions on Intelligent Transportation Systems*, vol. 20, no. 7, pp. 2593–2604, Jul. 2019, conference Name: IEEE Transactions on Intelligent Transportation Systems.

[5] A. Papalia, N. Thumma, and J. Leonard, "Prioritized Planning for Cooperative Range-Only Localization in Multi-Robot Networks," *arXiv:2109.05132 [cs]*, Sep. 2021.

[6] J. Cano and J. Le Ny, "Improving Ranging-Based Location Estimation with Rigidity-Constrained CRLB-Based Motion Planning," in *2021 IEEE International Conference on Robotics and Automation (ICRA)*, May 2021, pp. 5758–5764, iSSN: 2577-087X.

[7] N. Patwari, J. N. Ash, S. Kyperountas, A. O. Hero, R. L. Moses, and N. S. Correal, "Locating the nodes: cooperative localization in wireless sensor networks," *IEEE Signal Processing Magazine*, vol. 22, no. 4, pp. 54–69, Jul. 2005.

[8] N. Michael, M. M. Zavlanos, V. Kumar, and G. J. Pappas, "Maintaining connectivity in mobile robot networks," in *Experimental Robotics*. Springer, 2009, pp. 117–126.

[9] P. Yang, R. A. Freeman, G. J. Gordon, K. M. Lynch, S. S. Srinivasa, and R. Sukthankar, "Decentralized estimation and control of graph connectivity for mobile sensor networks," *Automatica*, vol. 46, no. 2, pp. 390–396, 2010.

[10] Z. Sahinoglu, S. Gezici, and I. Guvenc, *Ultra-wideband Positioning Systems: Theoretical Limits, Ranging Algorithms, and Protocols*. Cambridge University Press, 2008.

[11] Decawave, "DW1000 User manual, V2.18," 2017. [Online]. Available: https://www.decawave.com/dw1000/usermanual/

[12] A. Ledergerber, M. Hamer, and R. D'Andrea, "A robot self-localization system using one-way ultra-wideband communication," in *Proceedings of the IEEE/RSJ International Conference on Intelligent Robots and Systems (IROS)*. IEEE, 2015.

[13] V. Mai, M. Kamel, M. Krebs, A. Schaffner, D. Meier, L. Paull, and a. R. Siegwart, "Local Positioning System Using UWB Range Measurements for an Unmanned Blimp," *IEEE Robotics and Automation Letters*, vol. 3, no. 4, pp. 2971–2978, Oct. 2018, number: 4.

[14] J. Cano, G. Pagès, E. Chaumette, and J. Le Ny, "Clock and power-induced bias correction for UWB time-of-flight measurements," *IEEE Robotics and Automation Letters*, vol. 7, no. 2, pp. 2431–2438, 2022.

[15] B. Etzlinger and H. Wymeersch, "Synchronization and Localization in Wireless Networks," *Foundations and Trends® in Signal Processing*, vol. 12, pp. 1–106, Jan. 2018.

[16] R. Peng and M. L. Sichitiu, "Angle of Arrival Localization for Wireless Sensor Networks," in *2006 3rd Annual IEEE Communications Society on Sensor and Ad Hoc Communications and Networks*, vol. 1, Sep. 2006, pp. 374–382, iSSN: 2155-5494.

[17] I. Dotlic, A. Connell, H. Ma, J. Clancy, and M. McLaughlin, "Angle of arrival estimation using decawave DW1000 integrated circuits," in *2017 14th Workshop on Positioning, Navigation and Communications (WPNC)*, Bremen, Oct. 2017.

[18] S. M. Kay, *Fundamentals of Statistical Signal Processing: Estimation Theory*. Englewood Cliffs, NJ, USA: Prentice-Hall, 1993.

[19] F. Pukelsheim, *Optimal Design of Experiments*. SIAM, 2006.

[20] J. Cano and J. Le Ny, "Ranging-Based Localizability-Constrained Deployment of Mobile Robotic Networks," *arXiv:2202.00756 [cs]*, Feb. 2022, arXiv: 2202.00756.

[21] T.-S. Tay and W. Whiteley, "Generating Isostatic Frameworks," *Struct. Topology*, vol. 11, Jan. 1985.

[22] S. Zhao and D. Zelazo, "Bearing rigidity and almost global bearing-only formation stabilization," *IEEE Transactions on Automatic Control*, vol. 61, no. 5, pp. 1255–1268, 2015.

[23] D. P. Bertsekas, *Nonlinear programming*, 3rd ed. Belmont, MA: Athena Scientific, 2016.

[24] K. B. Petersen and M. S. Pedersen, "The Matrix Cookbook," Technical University of Denmark, Tech. Rep., 2012.

[25] D. Bertsekas, *Dynamic programming and optimal control: Volume I*. Athena scientific, 2012, vol. 1.